RSC Medicinal Chemistry

Accepted Manuscript

This article can be cited before page numbers have been issued, to do this please use: G. M P, N. Muruganandam, S. Govindarajan and B. Babu, *RSC Med. Chem.*, 2026, DOI: 10.1039/D6MD00300A.

ROYAL SOCIETY OF CHEMISTRY

rsc.li/medchem

View Article Online
DOI: 10.1039/D6MD00300A

ARTICLE

Triarylphosphonium-conjugated Sn(IV)-porphyrins for Antimicrobial Photodynamic Therapy: Impact of Substituents on Lipophilicity, Aggregation, and Photoantibacterial Activity

Received 00th January 20xx,
Accepted 00th January 20xx

DOI: 10.1039/x0xx00000x

Gayathri MP, [a] Nandhakumar Muruganandam,[b] Sutharsan Govindarajan,*[b] Balaji Babu*[a]

*Antimicrobial photodynamic therapy is an effecive approach to couteract bacterial infections that are not possible to be treated through antibiotics. In this study, three cationic Sn(IV) porphyrins bearing triaryl phosphonium substituents (**SnP1**, **SnP2**, and **SnP3**) were synthesized and evaluated as antibacterial photosensitizers (PS). All compounds exhibited efficient singlet oxygen generation with quantum yields (Φ_Δ) in the range of 0.72-0.78. Aggregation studies shows reduced aggregation of **SnP1** and **SnP2** than **SnP3**. Lipophilicity (log P) values indicated that **SnP2**, containing fluoro substituents, possesses balanced amphilic character favorable for effective bacterial uptake and antimicrobial activity. The photodynamic antibacterial activity (427 nm LED, 22 mW cm^{-2}) of **SnP1**, **SnP2** and **SnP3** was evaluated against Escherichia coli (E. coli) and clinical methicillin-resistant Staphylococcus aureus (MRSA). **SnP2** exhibited significant photoantimicrobial activity against both gram negative (E. coli) and gram positive (MRSA) with log reduction of 8.7 at 10 μM and 8.4 at 20nM, respectively. Overall, our study highlights the importance of structural tuning of lipophilicity and aggregation in enhancing the efficacy of Sn(IV)-porphyrin based photosenstizers.*

1. Introduction

The growing threat of antimicrobial resistance has prompted global health agencies to identify priority pathogens that require urgent therapeutic intervention. The World Health Organization recently released the Indian Priority Pathogen List (IPPL), which highlights several clinically significant bacteria.[1] Among these, *Escherichia coli (E. coli), Klebsiella pneumoniae*, *Acinetobacter baumannii* and *Pseudomonas aeruginosa* are recognized as critical priority pathogens. In addition, high-priority pathogens include *Staphylococcus aureus* (particularly MRSA), *Enterococcus* species, and *Salmonella* species (typhoidal and non-typhoidal).[1,2]

Although a wide range of antimicrobial strategies has been developed, there is still a critical need for treatment that can reduce or supress the antibiotic resistance. In this context, oxidative stress-based antimicrobial methods have attracted considerable attention.[3] These approaches generate reactive oxygen species (ROS) that damage key cellular components-leading to microbial cell death.[3,4] The multi-target oxidative action of aPDT minimizes resistance development, making it effective against multidrug-resistant pathogens.[5]

In aPDT, upon light absorption the photosensitizer (PS) undergoes electronic excitation from the ground state to a higher-lying excited state, subsequently transferring energy to molecular oxygen to generate ROS, its efficacy is governed by molecular design, which dictates absorption properties, excited-state dynamics, ROS yield, and interactions with microbial cells.[6] These ROS induce oxidative damage to key cellular components, resulting in irreversible cellular damage and microbial cell death. Among various classes of photosensitizers investigated to date, tin(IV)-based porphyrins represent one of the most versatile and widely studied scaffolds for photodynamic applications.[7] Sn(IV)-porphyrins with trans axial ligands inhibit π-π interaction of porphyrin macrocycles and minimize aggregation. In addition, Sn(IV)-porphyrins exhibit strong absorption in the visible region (420-440 nm), facilitates intersystem crossing (ISC) thereby populates triplet-state yields, and efficient singlet oxygen generation, making them highly suitable candidate for aPDT.[8] Moreover, the porphyrin macrocycle provides a chemically flexible scaffold that allows systematic modification of peripheral substituents to fine tune the physicochemical properties such as lipophilicity, aggregation behaviour, and interaction with microbial cells.

For antimicrobial applications, efficient interaction between the photosensitizer and microbial cell surfaces is a critical determinant of photodynamic activity. Bacterial cell envelopes typically possess a net negative charge, which favours the interaction of cationic photosensitizers through electrostatic attraction. As a result, cationic porphyrin derivatives have shown enhanced antimicrobial photodynamic activity due to improved binding and uptake by microbial cells.[9] However, increasing hydrophobicity to enhance membrane interaction can also promote aggregation in aqueous environments, which often reduces antimicrobial photodynamic efficiency due to self-quenching of excited states. Therefore, achieving a balanced combination of charge, lipophilicity, and molecular dispersion is essential for optimizing antimicrobial

[a]Department of Chemistry, SRM University-AP, India;
[b]Department of Biological Sciences, SRM University-AP, India.

photodynamic performance. The choice of wavelength of light to activate a photosensitizer largely depends on the depth of infection. Blue light is well suited for superficial or topical infections; while red light is preferred for deep infections as it has better tissue penetrating.[4,5] Porphyrins with an intense absorption (Soret band) in blue region of the spectrum is a well-suited candidate as photosensitizer for topical bacterial infections.

In this context, attaching triaryl phosphonium ($TArP^+$) moieties-can be a promising strategy for modulating the lipophilic nature and aggregation nature of the photosensitizers.[10] The positive charge on triaryl phosphonium group that can enhance interactions with microbial membranes through electrostatic interactions of negatively charged microbial membranes while simultaneously influencing the hydrophobic character of the photosensitizer. In the present study, we investigate a series of triaryl phosphonium conjugated Sn(IV)-porphyrin photosensitizers (**SnP1**–**SnP3**) (Fig. 1a) designed to modulate lipophilicity, aggregation behaviour, and antimicrobial photodynamic activity towards gram (-) negative *Escherichia coli* and a Gram (+) positive methicillin-resistant *Staphylococcus aureus* (MRSA). By correlating molecular structure with photophysical and biological properties, this work provides insights into the structure–activity relationships governing phosphonium-based porphyrin photosensitizers and highlights their potential as promising agents for antimicrobial photodynamic therapy.

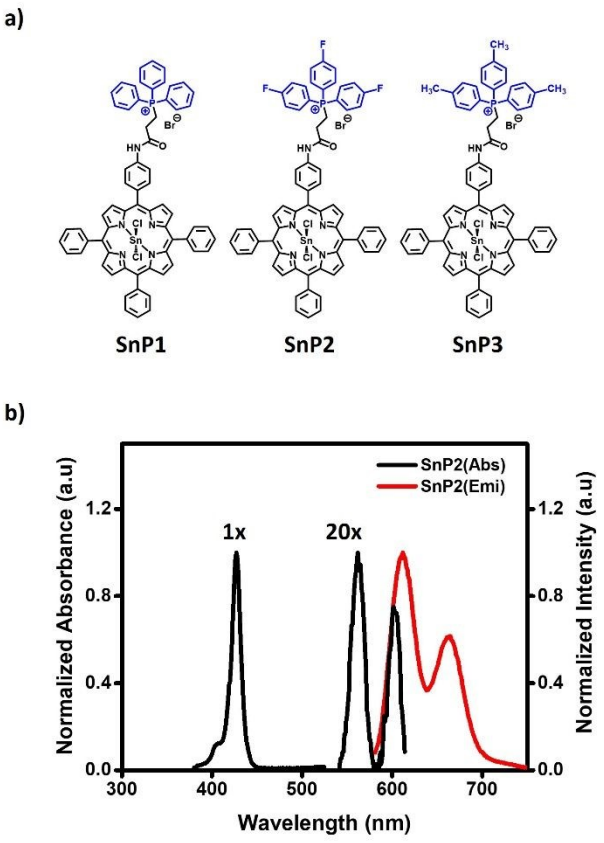

Fig. 1. (a) Schematic representation of Sn(IV) -porphyrins studied; (b) Absorption (black) and Emission (red) spectra of **SnP2** in DMF.

2. Results and Discussion

2.1. Synthesis and characterisation

The Sn(IV)-complexes (**SnP1**-**SnP3**) were prepared by stirring the corresponding free-base porphyrins[11] with $SnCl_2.H_2O$ at 60°C for 6h and purified by neutral alumina chromatography (Scheme S1). The structure of Sn(IV)-complexes were confirmed by NMR (^1H, ^{31}P, ^{19}F NMR) and Mass spectrometry (Figs. S1-S6). The β-hydrogens of porphyrin core were observed around 9.11 ppm, while the aryl protons of triarylphosphonium moiety appeared in the aromatic region (7.7-8 ppm). Signals corresponding to the aliphatic linker were detected around 3.2-3.5 ppm. The amide (NH) proton resonated downfield at 10.9 ppm consistent with reported literature values.[11] Furthermore, the ^{31}P-NMR of Sn(IV)-complexes showed characteristic peaks around 25 ppm which are downshifted from the free triaryl phosphines confirming successful conjugation (Figs. S1-S3). The ^{17}F-NMR of **SnP2** displayed fluorine peaks at -98.15 ppm. The mass spectral analysis revealed peaks corresponds to [M-2Cl+H] fragment.

2.2. Photophysical properties

The electronic absorption spectrum of Sn(IV)-porphyrins (**SnP1, SnP2** and **SnP3**) (Fig 1b and S7) show typical intense Soret band at 428 nm ($S_0 \rightarrow S_2$ transition) and two Q-bands around 563 and 605 nm ($S_0 \rightarrow S_1$ transition) typical of Sn(IV)-porphyrin systems.[12] All three Sn(IV)-porphyrins exhibited similar pattern in UV-Vis indicating the triarylphoshonium substitution have minimal impact on the electronic properties because of the aliphatic linkers. The emission spectra of Sn(IV)-porphyrins (**SnP1-SnP3**) displayed two emission bands around 610 and 662 nm when excited at 428 nm, the (Fig 1b and Fig S7). The fluorescence quantum yields (Φ_F) of Sn(IV)-porphyrins were low (0.029). The relatively low quantum yield values are consistent with typical Sn(IV)-porphyrin systems, where efficient intersystem crossing from the singlet excited state to the triplet state occurs.[13] The photophysical property results of all three compounds are mentioned in Table 1. The singlet oxygen generating ability of synthesised Sn(IV)-porphyrins were evaluated using 9,10-dimethylanthracene (DMA) as singlet oxygen trap.[14] DMA is also widely employed as a singlet oxygen probe. DMA reacts with singlet oxygen to form a stable endoperoxide, leading to a decrease in its characteristic absorption. Monitoring this decrease spectroscopically allows indirect detection and quantification of singlet oxygen generation by comparative method.[32] The singlet oxygen quantum yield (Φ_Δ) measurements indicate that all three Sn(IV)-porphyrins are efficient singlet oxygen generators upon irradiation. The control experiments in dark displayed negligible $^1O_2$ generation. The singlet oxygen ($^1O_2$) life-time is higher in organic solvents than in water and physiological environments. The fate of singlet oxygen is further governed by biomolecular quenching, oxygen availability, cellular microenvironment effects. Therefore, the measured Φ_Δ by DMA method primarily represents intrinsic photosensitising efficiency under idealized conditions and may not directly correlate with $^1O_2$ generation efficiency under physiological conditions.

View Article Online
DOI: 10.1039/D6MD00300A

Table 1. Selected photo physicochemical properties of **SnP1**-**SnP3** in DMF.

	SnP1	SnP2	SnP3
$\lambda_{max/nm}$ (log ε)	428 (5.11), 562(3.75), 605(3.66)	428(5.06), 563(3.70), 603(3.57)	428(5.10), 564(3.71), 605(3.61)
λ_{em}[a]	613, 662	612, 661	612, 662
Φ_F[b]	0.029	0.026	0.029
Φ_Δ[c]	0.72	0.78	0.76
log $P_{(o/w)}$	0.31	0.28	0.35

[a] Excitation at the B (or Soret) band maxima; [b] ZnTPP = 0.033 in DMF[16]; ZnTPP in DMF[30]

2.3. Aggregation studies

Porphyrins and metalloporphyrins tend to aggregate in aqueous or physiological medium due to either H or J- aggregation.[15] Sn(IV) porphyrins with suitable bulky trans-axial ligands are known to suppress H-aggregation by sterically hindering the close approach of adjacent porphyrin units, whereas those with simple axial ligands such as Cl or OH tend to exhibit some degree of aggregation in aqueous solution.[8] Aggregation significantly reduces the photodynamic efficiency of photosensitizers by quenching excited states and decreasing singlet oxygen generation.[17] Therefore, maintaining the photosensitizer in a monomeric form is essential for efficient ROS production and effective antimicrobial photodynamic therapy (aPDT). The aggregation behaviour of the three Sn(IV)-porphyrin derivatives (**SnP1**-**SnP3**) was evaluated by measuring their UV–visible absorption spectra in DMSO, 1% DMSO/PBS, and 1% DMSO/water (Fig. 2a-2c). In DMSO, all three compounds displayed a narrow and intense Soret band around 428 nm along with well-resolved Q-bands in the 520–610 nm region, suggesting that the Sn(IV)-porphyrins are present in a monomeric and well-dispersed form in this solvent. In 1% DMSO/H_2O, a slight blue shift (420nm) in soret band is observed for all three Sn(IV)-porphyrins, however, the band remained sharp with similar full-width-half-maximum (FWHM) value (Fig. 2d). Full-width-half-maximum (FWHM) is the width of a spectral peak measured at half of its maximum intensity, indicating peak sharpness and providing insight into aggregation and molecular environment.[7,8] This suggests that the Sn(IV)-porphyrins remains predominantly in monomeric form in 1% DMSO/H_2O. This behaviour is attributed to the cationic triarylphosphonium moiety which increases the solubility. Interestingly in 1% DMSO/PBS, for **SnP1** and **SnP2**, a decrease in soret band absorption is observed but the band remained narrow with

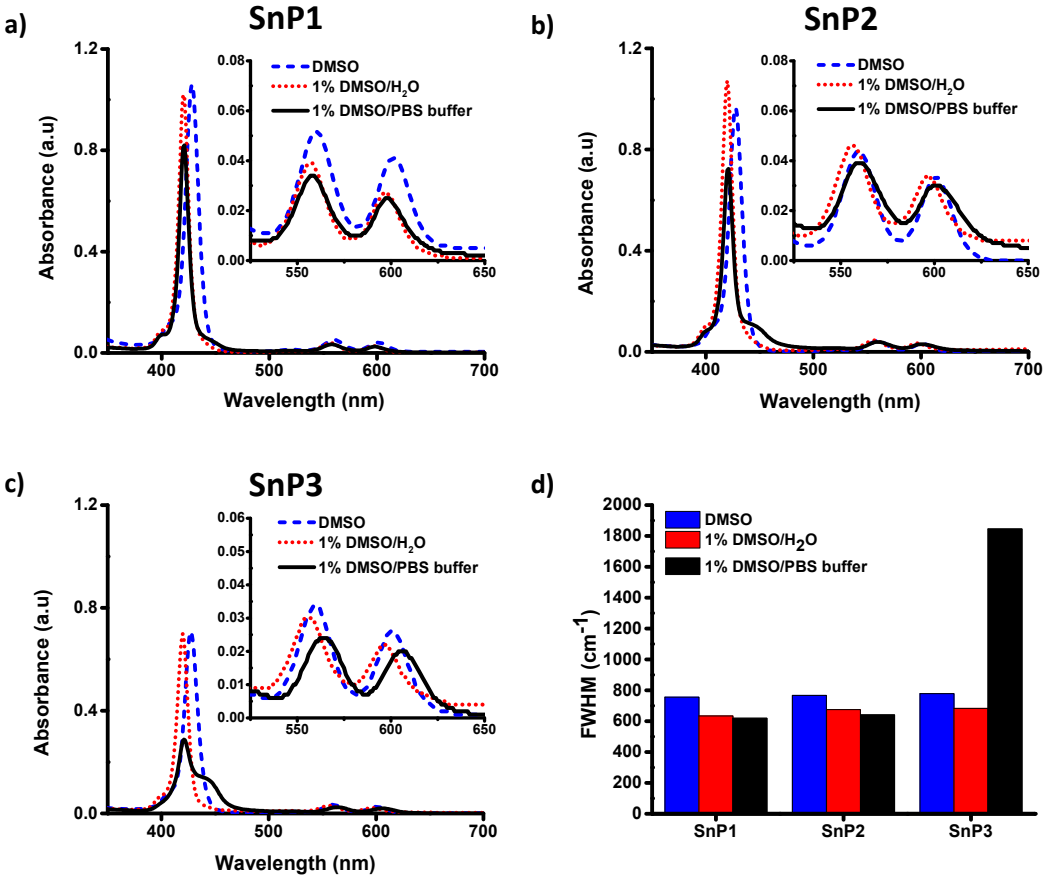

Fig. 2. Aggregation studies: UV-Visible spectra of a) **SnP1**, b) **SnP2**, c) **SnP3** in DMSO, 1% DMSO/H_2O, 1% DMSO/PBS buffer (Inset: Expanded Q-bands); d) FWHM (cm^{-1}) in DMSO (blue), 1% DMSO/H_2O (red) and 1% DMSO/PBS buffer (black).

DOI: 10.1039/D6MD00300A

similar FWHM. In case of **SnP3**, a significant decrease in soret band absorption is observed along with peak broadening. A new red shifted absorption band appeared with increased FWHM. This behaviour suggests that some degree of J-aggregation is induced for **SnP3** in 1% DMSO/PBS.[18] This is attributed to the increased hydrophobic nature contributed by tritolyphophonium moiety in **SnP3**, also the ionic strength in PBS aids in the reduction of solubility an increase of aggregation.[19] This study shows that how a small change in substituents on the triphenylphosphonium (TPP^+) moiety can strongly influence the aggregation behaviour of Sn(IV)-porphyrins because they alter steric and hydrophobic properties of the molecule.

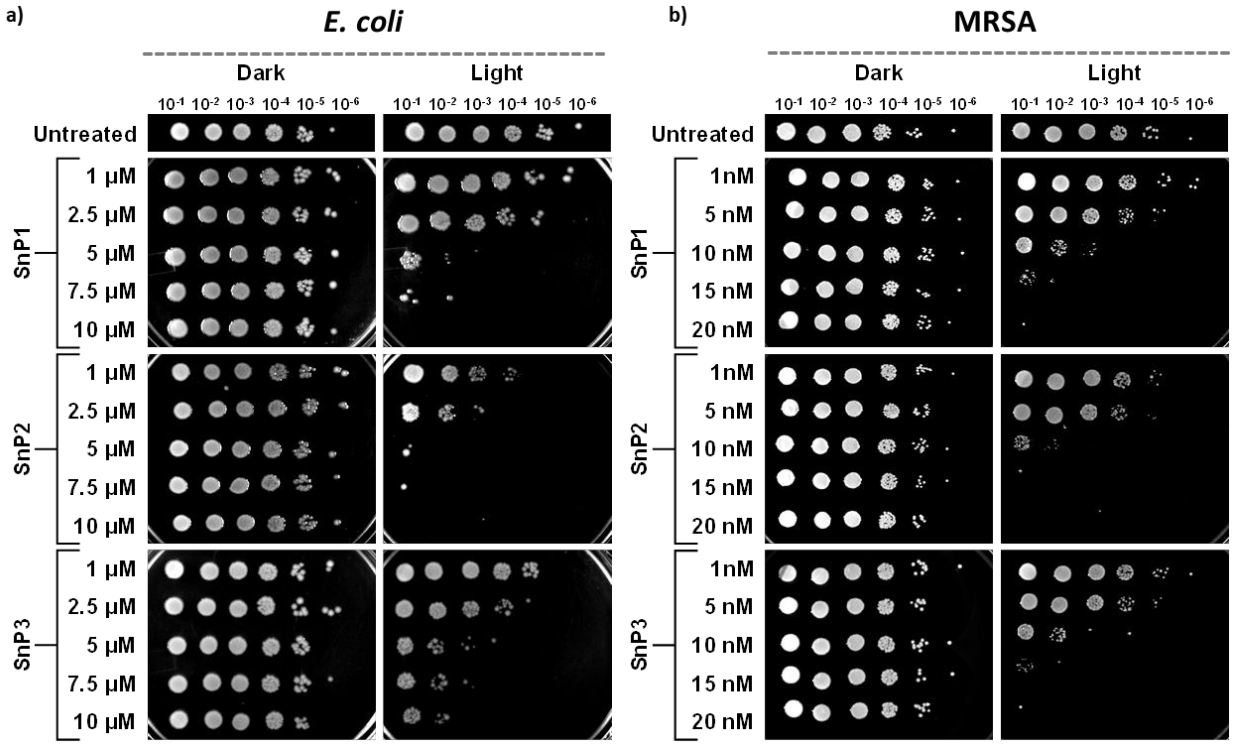

Fig. 3. Antibacterial activity of **SnP1**, **SnP2**, **SnP3** in dark and light exposure (427 nm LED, 30min 40 J cm^{-2}) conditions at different concentrations against (a) *E. coli*, (b) MRSA by spot dilution assay.

2.4. Lipophilicity

The uptake and interaction of porphyrins with bacterial membranes depends on the lipophilicity. This property directly influences antimicrobial photodynamic activity, as we have observed in our previous studies.[20] Balanced lipophilicity helps in minimizing aggregation and to maintain solubility. The lipophilicity of the synthesized Sn(IV)-porphyrin derivatives was evaluated by determining their octanol/water partition coefficients (log P) (Table 1).[21,29] The obtained values were 0.309 for **SnP1**, 0.283 for **SnP2**, and 0.347 for **SnP3**, indicating that all three compounds possess moderate lipophilicity with partial water solubility. Among the three derivatives, **SnP3** exhibits the highest logP value, which are likely due methyl substituents present in **SnP3** that increase its hydrophobicity. In contrast, **SnP2** shows the lowest logP value, likely due to the fluorine substituents, which slightly increase the polarity of the molecule and reduce its affinity for the organic phase. **SnP1** displays an intermediate logP value.

2.5. Photoantimicrobial activity against gram (-) *E. coli* and gram (+) clinical pathogen - MRSA

Blue-light absorbing photosensitizers are advantageous for treating skin bacterial infections because blue light (400–450 nm) penetrates sufficiently into superficial tissues not deep enough, where most skin infections occur.[22] Sn(IV)-porphyrins are ideal photosensitizers since they strongly absorb in the blue region (Soret band) and produce singlet oxygen efficiently. The antimicrobial photodynamic activity of the triaryl phosphonium-based photosensitizers **SnP1**-**SnP3** were evaluated against the *E. coli* (Gram -) and a clinical isolate of

Table 2. Log reduction of *E. coli* and MRSA treated with **SnP1**-**SnP3** with 10 µM and 20 nM respectively. In dark and 427 nm light irradiation (22 mW/cm^2, 40 J cm^{-2}) for 30 min.

Bacteria	Log reduction (% of survival)			Log reduction (% of survival)		
	Dark			Light		
	SnP1	**SnP2**	**SnP3**	**SnP1**	**SnP2**	**SnP3**
E. coli[a]	<0.1 (97.6)	<0.1 (95.3)	<0.1 (90.7)	8.6 (0)	8.7 (0)	3.7 (0)
MRSA[b]	<0.1 (91.1)	<0.1 (88.2)	<0.1 (91.1)	5.4 (0)	8.5 (0)	5.4 (0)

[a]10 µM and [b]20 nM of Sn(IV)-porphyrins.

View Article Online
DOI: 10.1039/D6MD00300A

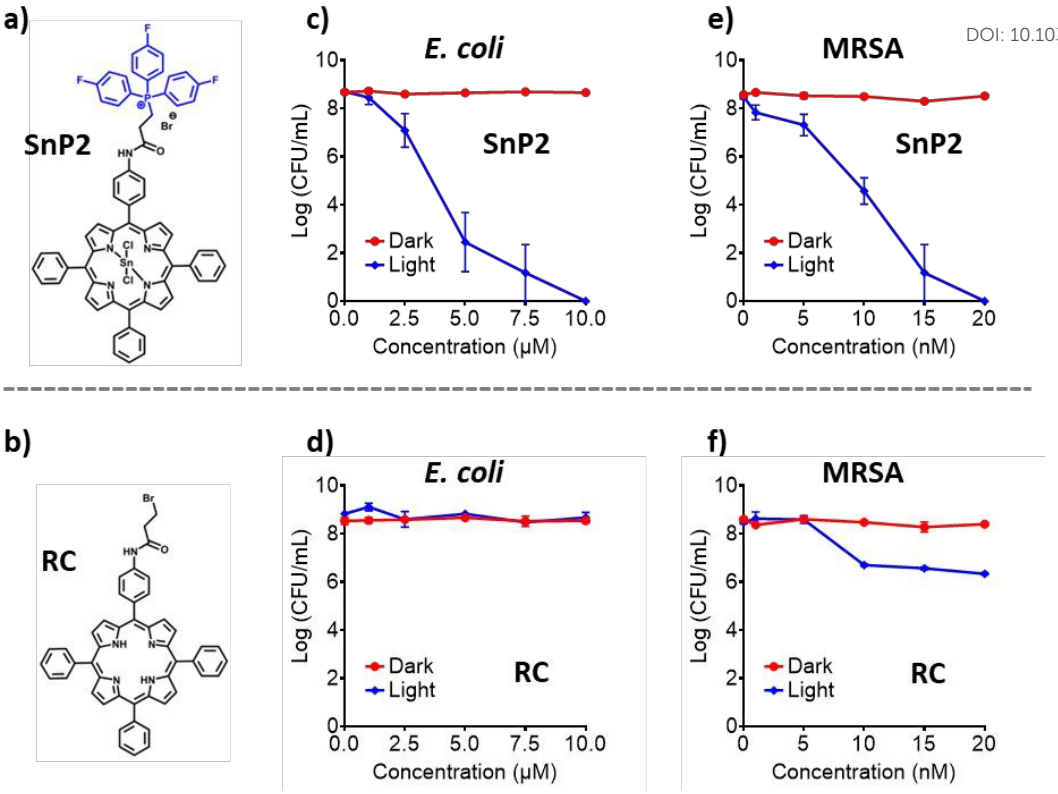

Fig. 4. Chemical structures and antibacterial activity of the compounds. (a) Reference compound (**RC**) (b) **SnP2**. Antibacterial activity against *E. coli* (c, d), against MRSA (e, f) under dark (red) and light irradiation with a 427 nm LED (22 mW cm^{-2}, 30min, 40 J cm^{-2}) (blue) conditions at different concentrations.

methicillin-resistant *S. aureus* (MRSA) (Gram +) (Fig. 3, 4 and S8). The Sn(IV)-porphyrins exhibited concentration dependent antibacterial activity under light exposure (427 nm LED). Significant differences in photoantibacterial efficacy were observed among the three compounds depending on the bacterial species. The log reduction numbers are calculated using the expression: log reduction = $\log_{10}(A_0)-\log_{10}(A_{30})$, where A_0 and A_{30} correspond to the number of viable microorganisms at 0 and 30 min of light exposure, respectively (Table 2). In accordance with established antimicrobial efficacy criteria, a log reduction exceeding 3 log units (≥99.9%) was deemed as the threshold for significant antibacterial activity.[31] In *E. coli*, **SnP1** and **SnP2** exhibited the highest photoantibacterial activity at 10 μM, with the log reductions of 8.7 for both the compounds. At 7.5 μM concentration, the log reductions are 4.13 and 5.65, respectively, for **SnP1** and **SnP2**. In contrast, **SnP3** showed lower photoantibacterial activity at the tested concentration, producing a log reduction of 3.7 at 10 μM. Interestingly, in

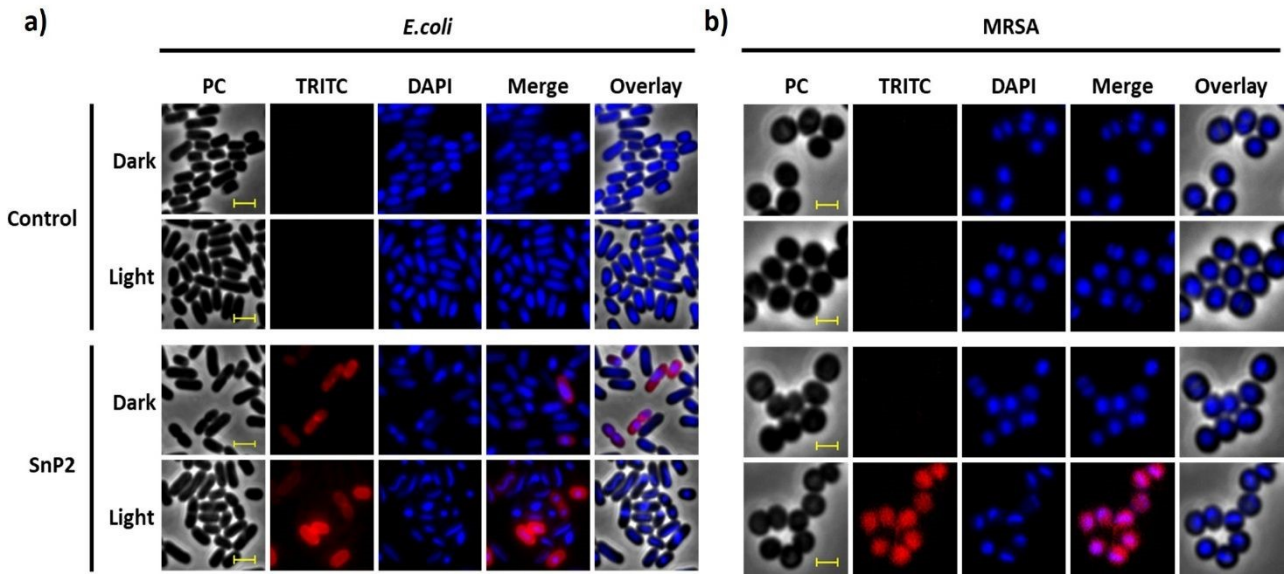

Fig. 5. Fluorescence microscopy images of (a) *E. coli* treated with 10 μM of **SnP2** in dark and after light exposure (427 nm LED, 22 mW cm^{-2}); (b) MRSA treated with 20nM of **SnP2** in dark and after light exposure (427 nm LED, 22 mW cm^{-2}). Localization of the **SnP2** compound was observed in the TRITC filter of fluorescence microscopy, and the cells were observed with phase contrast (PC). PC images (grey), DAPI (blue) and the compound fluorescence (Red) are shown in individual panels. The scale bar corresponds to 2 μm.

MRSA, these compounds exhibited strong photoantibacterial activity at nanomolar concentrations. **SnP1** and **SnP3** showed similar photoantibacterial activity at 20 nM (Fig. 3, S8), producing log reduction of 5.4, whereas **SnP2** exhibited the highest photoantibacterial activity with the log reduction of 8.49 and completely inhibited bacterial growth at 20 nM. Overall, among the three compounds, **SnP2** presents the highest aPDT activity followed by **SnP1** and **SnP3** (Fig. 4c, 4e). The difference in the aPDT activity between gram (-) compared to gram (+) could be explained due to the presence of an additional outer membrane in Gram-negative *E. coli*, which acts as a permeability barrier and may limit the uptake of the photosensitizers. [23] Consistent with their photoactivable nature, all the three Sn(IV)-porphyrins showed negligible aPDT at all concentrations tested against *E. coli* and MRSA in dark conditions. However, a notable feature of **SnP2** is that its light-activated antibacterial effects are more pronounced compared to Sn(IV)-porphyrins reported previously in the literature.[24] The low dark toxicity and high light induced toxicity are one of the main criteria for effective photosensitizers (PS) for aPDT. A control experiment with porphyrin-a reference compound (**RC**) (Fig. 4b) without triphenylphosphonium moiety showed negligible toxicity in dark and light in the same concentration range studied against *E. coli* and MRSA (Fig. 4d, 4f). The combined results of aggregation studies, singlet oxygen generation and light-induced toxicity collectively demonstrates that Sn(IV)-porphyrins (**SnP1**-**SnP3**) possess promising potential as photosensitizer for antimicrobial photodynamic therapy (aPDT).

2.6. Fluorescence Microscopy Localization Studies

Sn(IV)-porphyrins (**SnP1**-**SnP3**) are relatively emissive, and this property can be exploited to investigate their localisation and accumulation in bacterial cells under both dark and photodynamic conditions (Fig. 5, S9). Based on the toxicity profile in dark, fluorescence imaging studies were performed at 10 µM and 20 nM concentration of Sn(IV)-porphyrin for *E. coli* and MRSA, respectively. Fluorescence microscopic images of *E. coli* and MRSA were captured upon incubation with Sn(IV)-porphyrins along with DAPI-a DNA binding dye (Fig. 5, S9). Under dark conditions, photosensitizers were predominantly accumulated at the membrane, in addition to cytoplasmic localisation, of *E. coli*. However, in MRSA, a weak or no fluorescence signal was observed. In both cases DAPI staining revealed a smooth bacterial nucleoid morphology, similar to untreated control, indicating that Sn (IV)-porphyrins do not induce any DNA damages under dark conditions.

Upon light activation, Sn(IV)-porphyrin exhibited enhanced red fluorescence signal both in *E. coli* and MRSA. In both cases no visible damage to cell membrane was observed. However, DAPI staining showed a distorted and condensed nucleoid, indicative of photodynamic activation and DNA damage. Cells treated with **SnP1** and **SnP3** showed phenotypic changes similar to those observed with **SnP2** (Fig. S9). These red fluorescence signals indicate cellular uptake of the compounds. In *E. coli*, fluorescence was observed only in a subset of cells, whereas in MRSA nearly all cells exhibited strong fluorescence, suggesting more efficient uptake of the compounds by MRSA compared to *E. coli*. This observation correlates with the higher antimicrobial activity observed in MRSA relative to *E. coli*.

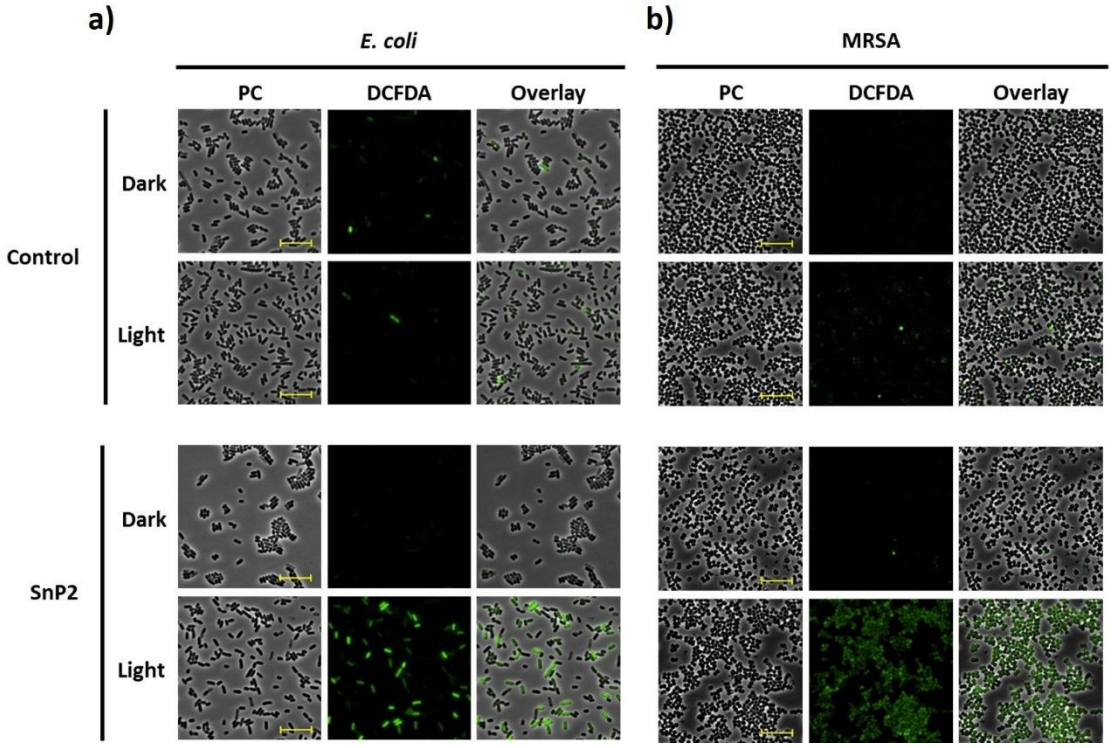

Fig. 6. DCFDA assay for intracellular ROS generation. Fluorescence microscopic images of (a) *E. coli* treated with 10 µM of **SnP2** in dark and light along with controls; (b) MRSA treated with 20 nM of **SnP2** in dark and light along with controls. Phase contrast (PC) (grey) and FITC filter (DCFDA) (green). The scale bar corresponds to 10 µm.

2.7. Intracellular ROS production

Next, we studied intracellular ROS generating ability of synthesized photosensitizers by DCFDA (2',7;-dichlorofluorescein diacetate) assay.[25] DCFDA is non-emissive cell-permeable dye undergoes deacetylation to form DCFH- a non-fluorescent intermediate. DCFH non-specifically react with any reactive oxygen species and oxidised to DCF (2',7;-dichlorofluorescein), a highly green emissive compound.[26] *E. coli* and MRSA were incubated with **SnP2** and DCFDA, and kept in dark and light conditions. The fluorescence microscopic images of bacteria (*E. coli* and MRSA) display no visible green emission from the cells kept in dark conditions. Interestingly a pronounced increase in green fluorescence was observed in bacteria preincubated with **SnP2** upon light exposure indicating efficient intracellular ROS generation. Control experiments in *E. coli* and MRSA in dark and light conditions in the absence of **SnP2** exhibited no detectable green fluorescence (Fig. 6). These results confirm that **SnP2** induces light-triggered ROS generation within the bacterial cells.

3. Conclusion

In conclusion, three triaryl phosphonium-substituted Sn(IV) porphyrins (**SnP1**, **SnP2**, and **SnP3**) were successfully synthesized and characterized. The influence of substituents on the triphenyl phosphonium groups was systematically investigated in terms of aggregation behaviour, lipophilicity, and antimicrobial photodynamic activity. Among the three compounds, **SnP2** exhibited the most balanced lipophilicity with reduced aggregation and enhanced antimicrobial activity against both *E. coli* and MRSA, highlighting the importance of structural modification in optimizing photodynamic efficiency. Thus, fine-tuning substituent effects on phosphonium porphyrins is an effective strategy for developing potent Sn(IV)-porphyrin based photosensitizers for antimicrobial photodynamic therapy. Further structural refinement of Sn(IV) porphyrins via *meso*-substitution can be strategically employed to enhance aqueous solubility, thereby enabling more comprehensive *in vitro* and *in vivo* evaluation. Moreover, the *trans*-dichloro axial coordination sites offer a synthetically accessible platform for ligand exchange, facilitating the incorporation of suitable axial ligand that can improve water solubility and enable the introduction of targeting moieties, ultimately enhancing cellular uptake and antimicrobial photodynamic efficacy.

4. Experimental

4.1. Materials

Benzaldehyde, Triphenylphosphine were obtained from Avra (India), Tris(4-fluorophenyl) phosphine, Tri(p-tolyl) phosphine and 2',7'-dichlorofluorescein diacetate (DCFDA) are from BLD pharma. 3-bromo-N-(4-(10,15,20-triphenylporphyrin-5-yl)phenyl) propenamide were synthesized according to literature procedures.[27,28] *E. coli* (MG1655) and methicillin-resistant *S. aureus* (MRSA) (ATCC43300) were used in this study. Bacterial strains were cultured in Lysogeny Broth (LB) and agar (1% tryptone (w/v), 0.5% yeast extract (w/v), 1% NaCl (w/v), 2% agar/pH 7.2) were employed. For antibacterial assays, LB agar plates were prepared with 2% agar. For all experiments bacteria were maintained at a temperature of 37 °C.

4.2. Methods

Detailed instrumentation and experimental protocols for bacterial work, fluorescence imaging and DCFDA studies are included in the ESI

4.3. Synthesis

The free base porphyrins (**P1**-**P3**) were synthesized by following the previously reported procedure (Scheme S1).[28] The respective free base porphyrins and $SnCl_2 \cdot H_2O$ were dissolved in dimethylformamide (DMF) and heated at 60 °C for 6h. The completion of reaction was monitored by TLC and UV-Vis spectra. Then the reaction mixture was added to ice-cold water to precipitate the compound. The precipitate was centrifuged and supernatant was discarded. The crude pellet was washed with water to remove the DMF and dried and purified by neutral alumina column chromatography (1% MeOH/$CHCl_3$) to give Sn(IV)-porphyrins (**SnP1**-**SnP3**) as purple solid in moderate yield.

SnP1. ^{1}H NMR ($CDCl_3$, 400 MHz): δ H 10.94 (s, 1H), 9.11 (m, 8H), 8.33 (dd, 6H), 8.19 (d, 2H), 8.01 (d, 2H), 7.76 (m, 24H), 3.75 (m, 2H), 3.24 (m, 2H); ^{31}P NMR ($CDCl_3$, 400 MHz): 23.87. MS (HRMS): m/z for [M−2Cl+H] = 1064.41 (calc. 1064.81). UV-Vis (λ/nm) in DMF: 428, 562, 605.

SnP2. ^{1}H NMR ($CDCl_3$, 400 MHz): δ H 10.64 (s, 1H), 9.11 (m, 8H), 8.32 (dd, 6H), 8.17 (d, 2H), 7.93 (d, 2H), 7.80 (m, 15H), 7.41 (m, 6H), 3.85 (m, 2H), 3.20 (m, 2H); ^{31}P NMR ($CDCl_3$, 400 MHz): 24.61; ^{19}F NMR ($CDCl_3$, 400 MHz): -98.15. MS (HRMS): m/z for [M-2Cl+H] = 1118.41 (calc. 1118.78). UV-Vis (λ/nm) in DMF: 428, 563, 603.

SnP3. ^{1}H NMR ($CDCl_3$, 400 MHz): δ H 10.95 (s, 1H), 9.12 (m, 8H), 8.34 (m, 6H), 8.19 (d, 2H), 8.09 (d, 2H), 7.84 (m, 9H), 7.64 (m, 6H), 7.54 (m, 6H), 3.63 (m, 2H), 3.20 (m, 2H), 2.50 (s, 9H); ^{31}P NMR ($CDCl_3$, 400 MHz): 25.01. MS (HRMS): m/z for [M-2Cl+H] = 1106.42 (calc. 1106.89). UV-Vis (λ/nm) in DMF: 428, 564, 605.

Author contributions

M.P.G contributed to synthesization of the molecules, photophysical properties, biological assays, writing-original draft, review and editing. N.M. contributed to biological assays, writing – review and editing. B.B. & S.G. contributed to conceptualization, methodology, investigation, supervision, writing – review and editing, funding acquisition, and resources.

Conflicts of interest

There are no conflicts to declare.

Data availability

The data supporting this article have been included as part of the Supplementary Information.

Acknowledgements

M.P.G. and N.M. thank SRM University-AP for Junior Research Fellowship and CSIR Direct-SRF respectively. The authors acknowledge SRM University-AP, Andhra Pradesh, for their instrumentation facilities. B.B. acknowledges seed funding from SRM University-AP (SRMAP/URG/SEED/2023-24/011) and DST-FIST [SR-FST-CS-I-2021-219(C)] for supporting the Department of Chemistry, SRM University-AP. S.G. acknowledges funding from DST-SERB (CRG/2020/003295) and SRM University-AP (SRMAP/URG/GENERAL-D/2025-26/007).

References

1 H. Sati, E. Carrara, A. Savoldi, P. Hansen, J. Garlasco, E. Campagnaro, S. Boccia, J. A. Castillo-Polo, E. Magrini, P. Garcia-Vello, E. Wool, V. Gigante, E. Duffy, A. Cassini, B. Huttner, P. R. Pardo, M. Naghavi, F. Mirzayev, M. Zignol, A. Cameron, E. Tacconelli, A. Aboderin, M. Al Ghoribi, J. Al-Salman, A. Amir, A. Apisarnthanarak, M. Blaser, A. El-Sharif, S. Essack, S. Harbarth, X. Huang, G. Kapoor, G. Knight, J. C. Muhwa, D. L. Monnet, T. Ousassa, R. Sacsaquispe, J. Severin, M. Sugai, N. Taneja and A. Umubyeyi Nyaruhirira, *Lancet Infect. Dis.*, 2025, **25**, 1033–1043.

2 M. E. A. de Kraker, A. J. Stewardson and S. Harbarth, *PLoS Med.*,2016, **13** (11), e1002184.

3 Á. Mourenza, J. A. Gil, L. M. Mateos and M. Letek, *Antioxidants 2020, **9 (5)***, 361.

4 M. J. Davies, *Biochem. Biophys. Res. Commun.*, 2003, **305**, 761–770.

5 G. Jori, C. Fabris, M. Soncin, S. Ferro, O. Coppellotti, D. Dei, L. Fantetti, G. Chiti and G. Roncucci, *Lasers Surg. Med.*, 2006, **38**, 468–481.

6 A. Anas, J. Sobhanan, K. M. Sulfiya, C. Jasmin, P. K. Sreelakshmi and V. Biju, *J. Photochem. Photobiol. C Photochem. Rev.*, 2021, **49**, 100452.

7 B. Babu, J. Mack and T. Nyokong, *Dalt. Trans.*, 2023, **52**, 5000–5018.

8 M. Ravikumar, D. Raghav, K. Rathinasamy, A. Kathiravan and E. M. Mothi, *ACS Appl. Bio Mater.*, 2018, **1**, 1705–1716.

9 I. O. Savelyeva, K. A. Zhdanova, M. A. Gradova, O. V. Gradov and N. A. Bragina, *Curr. Issues Mol. Biol.*, 2023, **45**, 9793–9822.

10 R. Bresolí-Obach, I. Gispert, D. G. Peña, S. Boga, Ó. Gulias, M. Agut, M. E. Vázquez and S. Nonell, *J. Biophotonics*, 2018, **11**, e201800054.

11 B. Babu, J. Mack and T. Nyokong, *New J. Chem.*, 2022, **46**, 5288–5295.

12 N. K. Shee and H. J. Kim, *Molbank 2023, Vol. 2023,* M1669.

13 J. Aaviksoo, A. Freiberg, S. Savikhin, G. F. Stelmakh and M. P. Tsvirko, *Chem. Phys. Lett.*, 1984, **111**, 275–278.

14 R. Bresolí-Obach, J. Torra, R. P. Zanocco, A. L. Zanocco and S. Nonell, *Methods Mol. Biol.*, 2021, **2202**, 165–188.

15 S. M. Safar Sajadi and S. Khoee, *Sci. Reports 2021 111*, **11**, 2832.

16 M. Taniguchi, J. S. Lindsey, D. F. Bocian and D. Holten, *J. Photochem. Photobiol. C Photochem. Rev.*, 2021, **46**, 100401.

17 K. Procházková, Z. Zelinger, K. Lang and R. Kubát, *J. Phys. Org. Chem.*, 2004, **17**, 890–897.

18 G. G. Parra, D. S. Correa, E. Silveira-Alves, L. M. Almeida, M. A. R. Souza, L. De Boni, L. Misoguti, C. R. Mendonça, S. C. Zílio, N. M. Barbosa Neto, I. E. Borissevitch and P. J. Gonçalves, *Spectrochim. Acta Part A Mol. Biomol. Spectrosc.*, 2021, **261**, 120063.

19 R. Koynova, B. Tenchov, L. Wang and R. C. MacDonald, *Mol. Pharm.*, 2009, **6**, 951.

20 A. Sułek, B. Pucelik, M. Kobielusz, A. Barzowska and J. M. Dąbrowski, *Int. J. Mol. Sci.*, 2020, **21**, 8716.

21 B. Babu, R. C. Soy, J. Mack and T. Nyokong, *New J. Chem.*, 2020, **44**, 11006–11012.

22 T. Dai, A. Gupta, C. K. Murray, M. S. Vrahas, G. P. Tegos and M. R. Hamblin, *Drug Resist. Updat.*, 2012, **15**, 223.

23 C. Maher and K. A. Hassan, *MBio*, 2023, **14**, e01205-23.

24 T. Goslinski and J. Piskorz, *J. Photochem. Photobiol. C Photochem. Rev.*, 2011, **12**, 304–321.

25 E. Eruslanov and S. Kusmartsev, *Methods Mol. Biol.*, 2010, **594**, 57–72.

26 D. Figueroa, M. Asaduzzaman and F. Young, *J. Pharmacol. Toxicol. Methods*, 2018, **94**, 26–33.

27 N. S. Lebedeva, Y. A. Gubarev, E. S. Yurina, E. N. Smirnova and S. A. Syrbu, *Colloid Polym. Sci. 2017 29511*, 2017, **295**, 2173–2182.

28 H. Koga, T. Hamada and S. Sakaki, *Dalt. Trans.*, 2003, 1153–1160.

29 J. X. Soares, Á. Santos, C. Fernandes and M. M. M. Pinto, *Chemosensors*, 2022, **10 (8)**, 340.

30 R. Bresolí-Obach, J. Torra, R. P. Zanocco, A. L. Zanocco and S. Nonell, *Methods Mol. Biol.*, 2021, **2202**, 165–188.

31. E. Alves, MAF. Faustino, M. G. Neves, A. Cunha, J. Tome, A. Almeida, *Fut Med Chem.* 2014, **6**, 141–164.

32. W. Li , L. Li , H. Xiao , R. Qi , Y. Huang , Z. Xie , X. Jing and H. Zhang, *RSC Adv.*, 2013, **3**, 13417-13421.

View Article Online
DOI: 10.1039/D6MD00300A

The data supporting this article have been included as part of the supplementary information (SI).

Supplementary information is available.